

# Cascaded four-wave mixing generation in photonic crystal fibers

Jing Hou · Ying Li · Jinyong Leng ·  
Pu Zhou · Zongfu Jiang

Received: 6 April 2013 / Accepted: 9 May 2013 / Published online: 21 June 2013  
© Springer-Verlag Berlin Heidelberg 2013

**Abstract** We investigate the efficient generation of broadband cascaded four-wave mixing products seeded at different wavelengths in photonic crystal fibers, with a high-peak power picosecond pulse pumping in the anomalous dispersion region as well as the normal dispersion regime. Multiple four-wave mixing products with different frequency intervals have been experimentally achieved when pumping in the anomalous dispersion region. Measured results present bandwidths of over 500 nm. We have also experimentally demonstrated that only seeding at the Stokes or anti-Stokes peaks can we get the efficient generation of cascaded four-wave mixing or cascaded stimulated Raman scattering when pumping in the normal dispersion regime.

## 1 Introduction

Four-wave mixing (FWM) in the continuous wave (CW) or long-pulse pump regime is one of the most fundamental nonlinear processes in optical fibers, in which two pump photons are annihilated and a signal photon and an idler photon are created [1]. This will produce when the phase-matching conditions are satisfied [1, 2]. In the absence of initial seeding (e.g., a CW signal), FWM creates symmetric spectral sidebands from noise. In the time domain, it leads to the generation of ultrafast pulses with temporal and amplitude modulation. This process is referred to as modulation instability (MI). So FWM and MI are simply

frequency-domain and time-domain instability descriptions of the same physics. Since the observation of MI in anomalous dispersion regime of single-mode optical fibers [3], a number of reviews have discussed the important nonlinear process during the supercontinuum generation [2, 4, 5]. And recently, research efforts have also been focused on the generation of cascaded FWM or MI. Because the cascaded FWM has great potential for innovations (e.g., frequency comb for metrology applications [6, 7]) and applications including multi-wavelength source for DWDM systems, generation of a soliton train at high repetition rates [3, 8].

In the year of 2006, experiments [8] reported a multiple FWM bandwidth of 90 nm in optical fibers. In their experiments or simulations, two CW signals were applied. Cascaded FWM products were also generated in the experiments of Ref. [7], by pumping two strong waves. And in 2009, Goëry Genty [9] numerically demonstrated the cascaded FWM in a photonic crystal fiber (PCF), in which a high-power picosecond pulse with modulated envelope was used. And recently, efficient generation of broadband four-wave mixing cascades centered at 1  $\mu\text{m}$  was first generated in a PCF with two zero-dispersion wavelengths (ZDWs), which was pumped by a two-tone seed [10]. Most results mentioned above were achieved by pumping in the anomalous dispersion regimes or near the ZDWs of the fibers.

We have also reported [11] efficient generation of Raman or FWM sidebands in an index-guided photonic crystal fiber, pumping in the anomalous dispersion region with a high-peak power pulse at 1,064 nm and a CW Stokes signal at 1,117 nm seeded. In this manuscript, we experimentally and numerically investigate cascaded FWM sidebands in PCFs seeded at different wavelengths, with pulse pumping in the anomalous dispersion region as well

---

J. Hou (✉) · Y. Li · J. Leng · P. Zhou · Z. Jiang  
College of Optoelectronic Science and Engineering,  
National University of Defense Technology, Changsha 410073,  
Hunan, People's Republic of China  
e-mail: houjing25@sina.com

as the normal dispersion regime. By performing the nonlinear experiments and simulations, we demonstrate that it is much easier to achieve broadband FWM sidebands with different frequency intervals when the high-peak power pulse pumps in the anomalous region. While only the Raman sidebands with frequency interval of  $\sim 13.4$  THz can be efficiently generated when pumping in the normal dispersion region and seeding at the Stokes or anti-Stokes peaks.

## 2 Experimental setup and fiber properties

The experimental setup is illustrated in Fig. 1, in which two signals were used, a CW signal (seed) and a pulse signal (pump). A 300 mW laser diode (LD) centered at 976 nm provides the pump of CW Stokes signal generator. An around 8 m, single-mode Yb-doped fiber (YDF) works as the gain medium which exhibits  $7.5 \mu\text{m}$  mode field diameter at 1,117 nm and 250 dB/m absorption at 976 nm. Three pairs of fiber gratings centered on 1,117, 1,034 and 1,040 nm were used as the faces of resonant cavity. Each pair contains one with higher reflectivity of  $\sim 99\%$  (HR) and one with lower reflectivity of  $\sim 30\%$  (LR). An optical isolator (ISO) was following to suppress optical reflection. And a long-pass filter ( $\sim 20$  nm) centered on 1,120 nm was placed after the ISO to eliminate pump light and other background lights when we got the 1,117 nm CW signal. Maximum average power of the CW signal can reach as  $\sim 100$  mW. The pulse signal was provided by a Nd:YAG Q-switched microchip laser (Teem Photonics, NP-10820), which is running at 1,064 nm and emitting 0.6 nm (FWHM) pulses with 15 kW peak power at a 7.3 kHz repetition rate supplies the other input of WDM by a simple  $25\times$  microscope objective. The free-space coupling efficiency (from laser to the input end of WDM) was about 40%. The pulse signal and the CW signal were combined with a WDM. Figure 2 shows spectra of the pulse at 1,064 nm and CW signals at 1,117, 1,040, 1,034 nm measured at the common port of WDM. Measuring resolution was set to 0.1 nm. The 3 dB spectral widths of the pulse or signals are smaller than 0.2 nm. The weak intensity near 1,064 nm in Fig. 2c, d comes from the low reflectance of the reflective port of WDM. In the following experiments we used two PCFs (fiber A and fiber B) with hexagonal lattice geometry, calculated dispersion profiles and effective mode field area (MFA,  $A_{\text{eff}}$ ) from a fully vectorial finite element mode solver (Comsol Multiphysics) displayed in Fig. 3. The hole-to-hole spacing  $\Lambda$  of fiber A is around  $5.42 \mu\text{m}$ , the average hole diameter  $d$  is  $3.54 \mu\text{m}$ , leading to a core diameter approximately equal to  $7 \mu\text{m}$ . For its larger diameter and appropriate ZDW at 1,117 nm, it has been used in the experiments of high-

power supercontinuum generation [12–14]. Fiber B has a core diameter of  $4.6 \mu\text{m}$ , hole-to-hole spacing  $\Lambda$  around  $3.35 \mu\text{m}$ , relative air hole diameter  $d/\Lambda = 0.61$ . Due to its smaller core diameter, fiber B exhibits a smaller MFA and therefore stronger nonlinearity than fiber A. Besides, its ZDW locates at 1,010 nm. This 1,064 nm high-power (kW) long pulse is in the anomalous dispersion regime and near ZDW. This would be conducive to the generation of cascaded FWM (or MI) sidebands [9, 15]. Although, the MFAs are both mismatched with that of HI1060 (the pigtail fiber of WDM), after optimizing the splicer parameters and controlling hole collapse of PCFs [16], we got the 90% coupling efficiency from WDM to fiber A and 70% coupling efficiency from WDM to fiber B. The spectra after the PCF were monitored with an optical spectrum analyzer (OSA) operating in the range of 600–1,700 nm.

## 3 Experimental results and discussion

In order to investigate the influence of ZDW to the efficient generation of cascaded FWM in index-guided PCFs, we used two PCFs with the ZDWs longer (fiber A) or shorter (fiber B) than the pulse pumping wavelength (1,064 nm). Therefore, this section is divided into three parts: the first part is focusing on the results generated in fiber A; the second part presents the generation of FWM products achieved in fiber B; and the third gives the discussion on the experimental results.

### 3.1 Pulse pumping in the normal dispersion regime (using fiber A)

This subsection is focusing on the generation of cascaded FWM products obtain by using fiber A. In a first step, we launched only the 1,064 nm pulse signal at different power levels into fiber A. The generated spectra in this pumping case are depicted in Fig. 4 with the measuring resolution

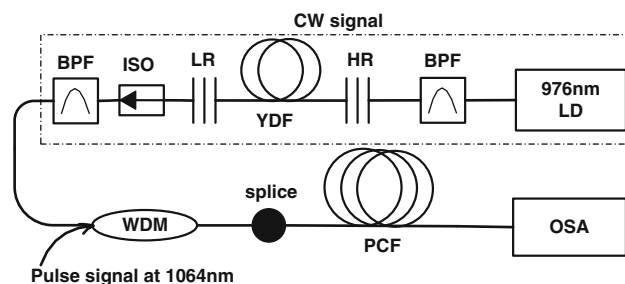


**Fig. 1** Schematic experimental setup. LD laser diode, BPF bandpass filter, HR fiber grating with higher reflectivity, YDF ytterbium-doped fiber, LR fiber grating with lower reflectivity, ISO isolator, PCF photonic crystal fiber, OSA optical spectrum analyzer

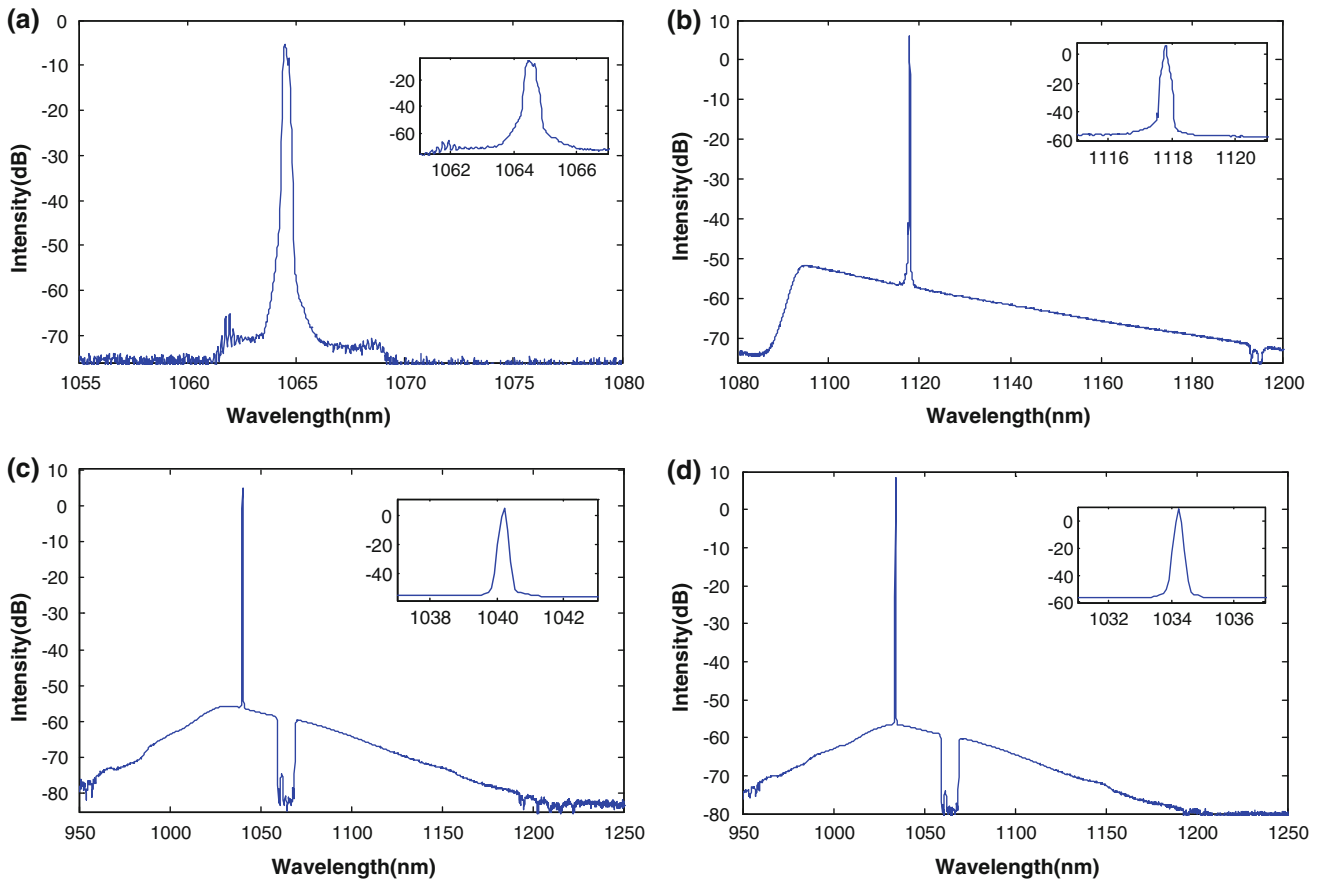


**Fig. 2** Measured spectra of pulse signal at 1,064 nm (a), and CW signals at 1,117 nm (b), 1,040 nm (c), 1,034 nm (d) with measuring resolution of 0.1 nm. *Insets* are the enlarged spectra

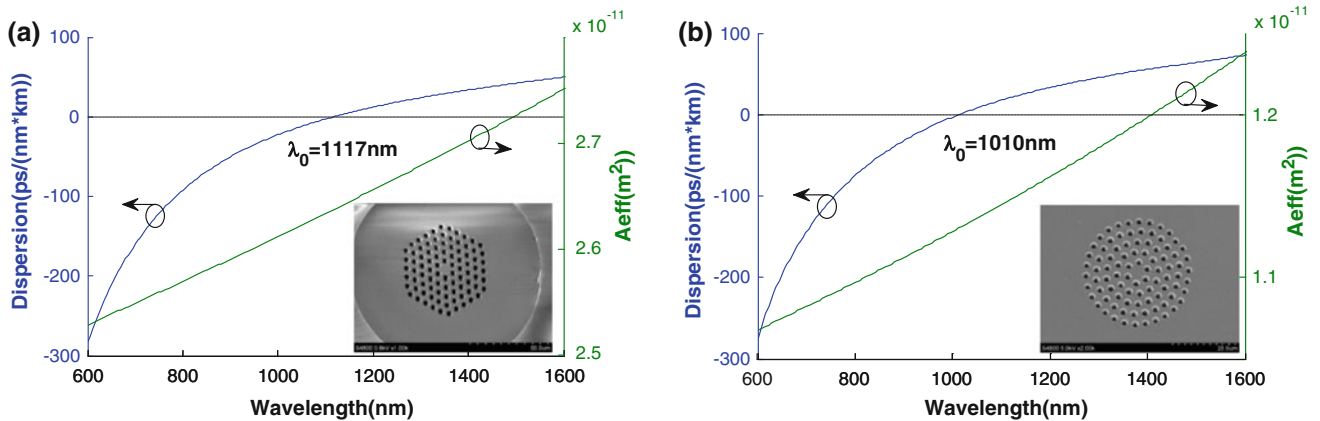


**Fig. 3** a Calculated dispersion and effective mode field area for fiber A. b For fiber B, dispersion and effective mode field area are calculated. The *insets* show SEM pictures of the respective fiber cross sections

of 1 nm. The profiles are not so smooth; this is due, in part, to the lack of resolution. A longer fiber length of 8 m (Fig. 4a) and a shorter fiber length of 1.5 m (Fig. 4b) were selected. Notably, all the spectra have a hump centered 1,117 nm (indicated by S1), which is easily recognized as the Stokes shift of the stimulated Raman scattering for

fused silica. And cascaded stimulated Raman scattering (SRS) generated high-order Stokes peaks (S2, S3) as well as anti-Stokes peaks (AS1, AS2) with the help of FWM. In Fig. 4b, the peak at 747 nm was generated by phase-matched degenerate FWM, as described in Ref. [17]. And the idler wave has a wavelength longer than 1,800 nm,

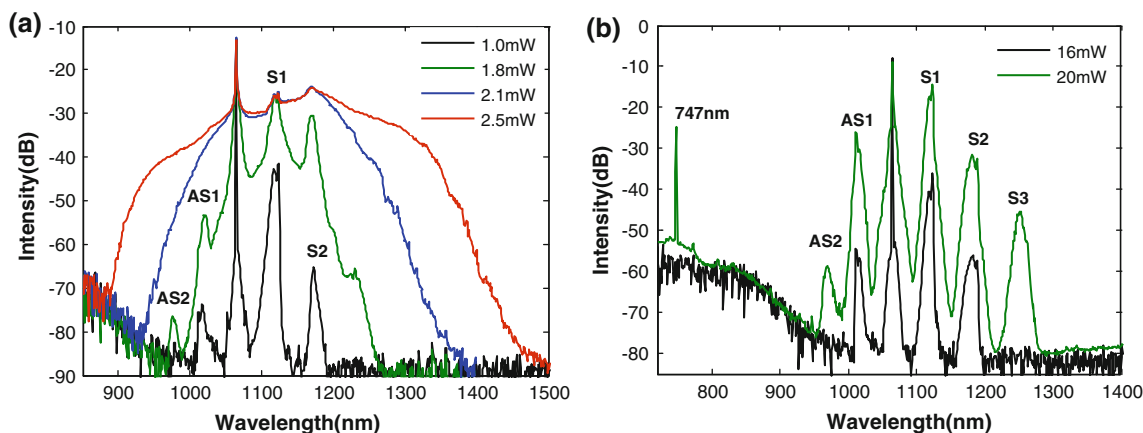


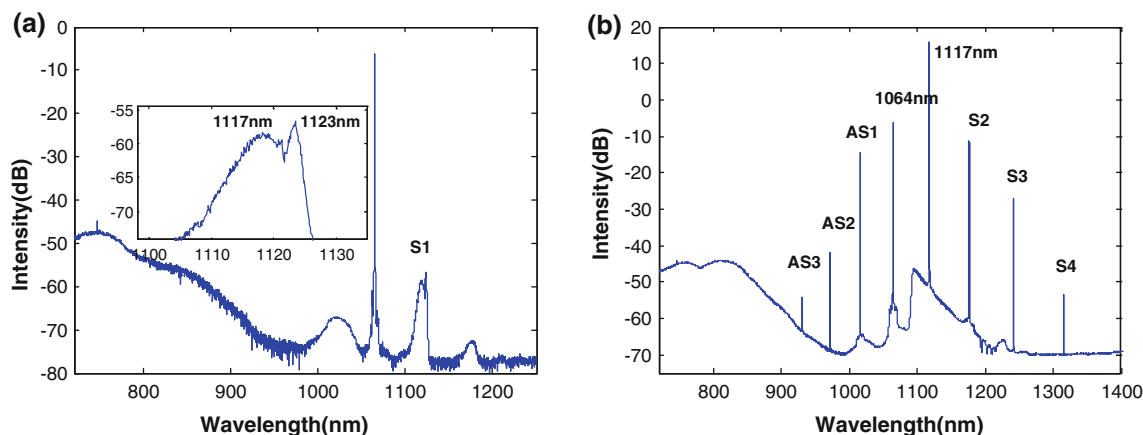
**Fig. 4** Spectra for only pulse pumping in fiber A with different power at the length of 8 m (a) and 1.5 m (b). Measuring resolution was set to 1 nm

which has exceeded the measuring range of our OSA at hand. So it cannot be observed. When fiber length was 8 m, power of pump pulse was largely consumed before it was strong enough to satisfy the phase-matching condition. So the degenerate FWM cannot be generated, although 8 m is much shorter than walk-off length [1]. Our results therefore show that the spectral broadening of the pulse in fiber A is mostly caused by cascaded stimulated Raman scattering.

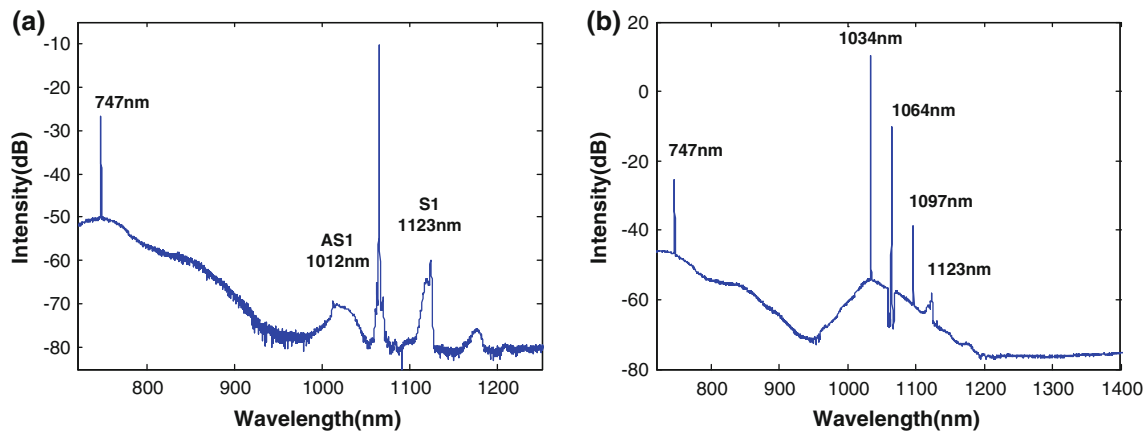
In a second step, we added a CW signal at 1,117 nm to perform the experiments. At this time, fiber length was selected as 1 m. Figure 5 shows the spectra of broadband Raman sidebands when CW signal with 55 mW was added (Fig. 5b), as well as the spectral profile for only pulse pumping (Fig. 5a). In the two figures, measured pulse average powers at the output of fiber A were both 20 mW. In Fig. 5a, the spectrum of Stokes peak of SRS was found to exhibit a double-peak structure corresponding to two peaks at 1,117 and 1,123 nm as shown in the inset of

Fig. 5a. So when we seed at the maximum of the Raman gain, double-peak structure evolved into the one-peak structure. At the same time, higher order Stokes peaks (indicated by S2, S3, S4 in Fig. 5b) were generated by cascaded SRS. This further promoted the generation of anti-stokes peaks (indicated by AS1, AS2, AS3 in Fig. 5b) with the help of FWM.

We then study how the sidebands can be affected if the seeding wavelength was tuned to 1,034 nm, which was far away from the first anti-Stokes peaks. Similarly, the spectrum of only pulse pumping is illustrated in Fig. 6a, with pulse power of 27 mW and fiber length of 1 m. Figure 6b shows the spectrum when a CW signal at 1,034 nm was added. However, we found that in this case, the resulting FWM sidebands were not so perfect as the case of seeding at 1,117 nm. As seen clearly in Fig. 6b, only one newly generated peaks at 1,097 nm can be observed. Compared with Fig. 6a, intensity of 747 nm was decreased. This is due to the consuming of pulse power by



**Fig. 5** Measured spectra for 20 mW only pulse pumping (a) and 55 mW CW signal at 1,117 nm (b) was added, with measuring resolution of 0.1 nm



**Fig. 6** Measured spectra for 27 mW only pulse pumping (a) and 45 mW CW signal at 1,034 nm (b) was added, with measuring resolution of 0.1 nm

the degenerate FWM, which generated the photons at 1,034 and 1,097 nm.

### 3.2 Pulse pumping in the anomalous regime (using fiber B)

In a second set of experiments, we recorded the FWM sidebands seeded at different wavelengths in fiber B. As described in [2, 15], FWM or MI is one of the most fundamental processes when long-pulse wave pumping in the anomalous dispersion regions. As a result, we first study the impacts of the pulse pump power on MI gain spectra. MI is the time-domain descriptions of the same physics as FWM [2]. And for MI gain spectrum  $g(\Omega)$ , taking into account the Raman response function, is given by [4, 18]

the Raman response function  $h(t)$  where  $\tau_1 = 12.2$  and  $\tau_2 = 32$  fs.

Figure 7 shows how the MI gain spectrum in fiber B changes with the pulse average power. From the bottom to the top, pulse average power increases from 2 to 16 mW in steps of 2 mW. And the locations of the maximum gain have been indicated. When the pump power is increased to 16 mW, the spectrum will get the maximum gain at 1,117 nm, which is the location of Raman shift.

As discussed in the preceding section, SRS dominates when the pulse pumps in the normal dispersion region. Here we have also recorded the spectral broadening in the early stage when pumping in the anomalous dispersion region. As shown in Fig. 8, spectra were generated from only pulse pumping in fiber B at different fiber lengths as

$$g(\Omega) = \text{Im} \left( \sqrt{ \pm \left[ \sum_{m=1}^{\infty} \frac{\beta_{2m}}{(2m)!} \Omega^{2m} + 2\gamma P_0 (1 - f_R + f_R \tilde{h}) \right] \sum_{m=1}^{\infty} \frac{\beta_{2m}}{(2m)!} \Omega^{2m} } \right) \quad (1)$$

where  $\Omega$  is the angular frequency offset relative to the pump.  $\beta_m = \partial^m \beta / \partial \Omega^m |_{\Omega=0}$  where  $\beta$  is the propagation constant,  $\gamma = n_2 \cdot \omega_0 / c \cdot A_{\text{eff}}$  is the nonlinear parameter,  $n_2 \cong 3 \times 10^{-20} \text{ m}^2/\text{W}$ , is the nonlinear refractive index of fused silica glass,  $\omega_0$  is the center frequency,  $P_0 = P_{\text{average}} / (t_{\text{FWHM}} \cdot \nu)$  is the peak power,  $P_{\text{average}}$  is the average pump power,  $t_{\text{FWHM}}$  the pulse full width at half maximum  $\nu$  is the repetition rate  $f_R = 0.18$  is the fractional contribution of the delayed Raman response.  $\tilde{h}(\Omega) = (\tau_1^2 + \tau_2^2) / (\tau_2^2 - \tau_1^2(i + \tau_2 \Omega)^2)$  is the Fourier transform of

well as different power levels for comparison. Each spectrum has a shape characteristic of cascaded MI. At the fiber length of 0.4 m (Fig. 8a), we recorded the spectra when the pump power was larger than 8 mW. While at the fiber length of 1 m (Fig. 8b), spectral bandwidth will be easily widened. So only the spectra with the pump power smaller than 3.5 mW were measured. Measuring resolution for Fig. 8a was 1 nm, and that for Fig. 8b was set to 0.1 nm. Inset in Fig. 8a is shown the enlarged spectra of the first Stokes peak at the power level of 11.5 mW with the measuring resolution 0.02 nm. The double-peak structure

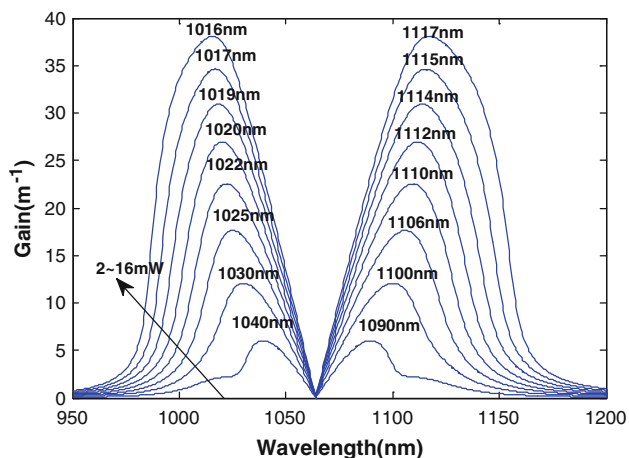


**Fig. 7** MI gain spectra in fiber B with pump power ranging between 2 mW and 16 mW in steps of 2 mW

can be observed clearly. The first peak locates at  $\sim 1,114$  nm, the second one happens at 1,123 nm. This was the combined effect of both the MI and SRS. With the pump power increasing to 16 mW in Fig. 8a, the maximum MI gain moved to  $\sim 1,116$  nm, which has a good coincidence with the calculations in Fig. 7. Results in Fig. 8 illustrate that a shorter fiber will generate larger-frequency-shift Stokes or anti-Stokes peaks with higher pulse pump power, while using a longer fiber will get smaller-frequency-shift Stokes or anti-Stokes peaks but with lower pulse pump power. As described in Ref. [11], seeding the CW signal at the Stokes peaks or anti-Stokes peaks is a good way to get pure FWM sidebands with a weak basement. So it is achievable to generate pure FWM sidebands with different frequency intervals, as long as the fiber length and pump power are suitably selected.

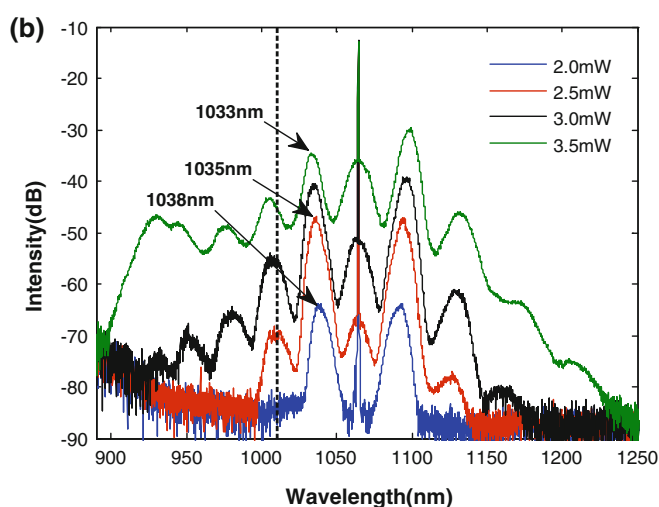
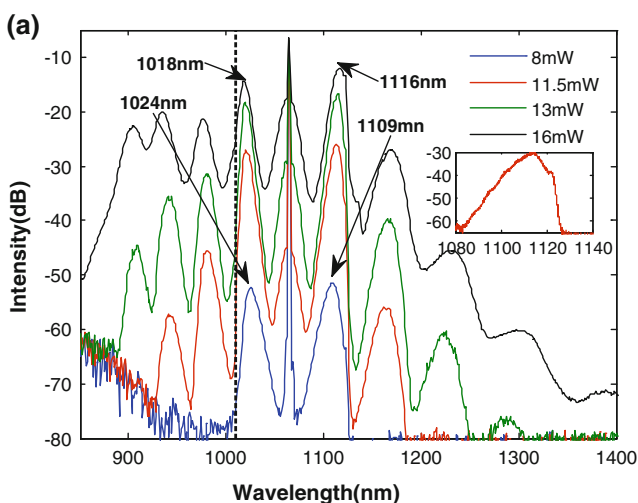


**Fig. 8** Measured spectra of only pulse pumping at different power levels in fiber B. The fiber length for **a** is 0.4 m, and that for **b** is 1 m; *inset* the measured first Stokes peak at the power level of 11.5 mW with a higher resolution. *Dashed lines* the locations of ZDW

Figure 9 displays the generation of cascaded FWM products seeded at different wavelengths. During the experiments, four CW signals with the wavelengths at 1,117, 1,034, 1,040 and 1,029 nm were used. The first three signals were achieved by the setup displayed in Fig. 1. And the CW signal centered on 1,029 nm was delivered by a laser diode with the maximum output power  $\sim 70$  mW. Through the calculations above we know that a pulse pump power of  $\sim 16$  mW will push first Stokes peak (generated by MI) to 1,117 nm. In order to get a spectrum with a shape characteristic of cascaded MI not a significantly widened supercontinuum when pumping by only pulse (see the dashed line Fig. 9a), the fiber length was selected as short as 0.4 m. After seeding near the first Stokes peak, FWM products spanning over 500 nm were generated (see the solid line in Fig. 9a).

Similarly, the fiber with the length of 1.5 m was used to realize the cascaded FWM products seeded at 1,034 and 1,040 nm. As shown in Fig. 8b, first anti-Stokes peak (generated by MI) locates at 1,034 nm provided the pulse pump power  $P_{\text{pulse}} \sim 3$  mW. Pure FWM sidebands were generated with pulse power 2.8 mW and seeded by 30 mW CW signal at 1,034 nm (see the solid line in Fig. 9b). When the CW wavelength was tuned to 1,040 nm as displayed in Fig. 9c, FWM sidebands can also be achieved but with a higher intensity basement.

Finally, fiber was cut to 1.3 m and pulse pump power was increased to 4.2 mW. The first anti-Stokes peaks for only pulse pumping located at 1,031 nm as indicated by the arrows in Fig. 9d. So seeding at 1,029 nm is suitable to the efficient generation of cascaded FWM, as displayed by the solid line in Fig. 9d.

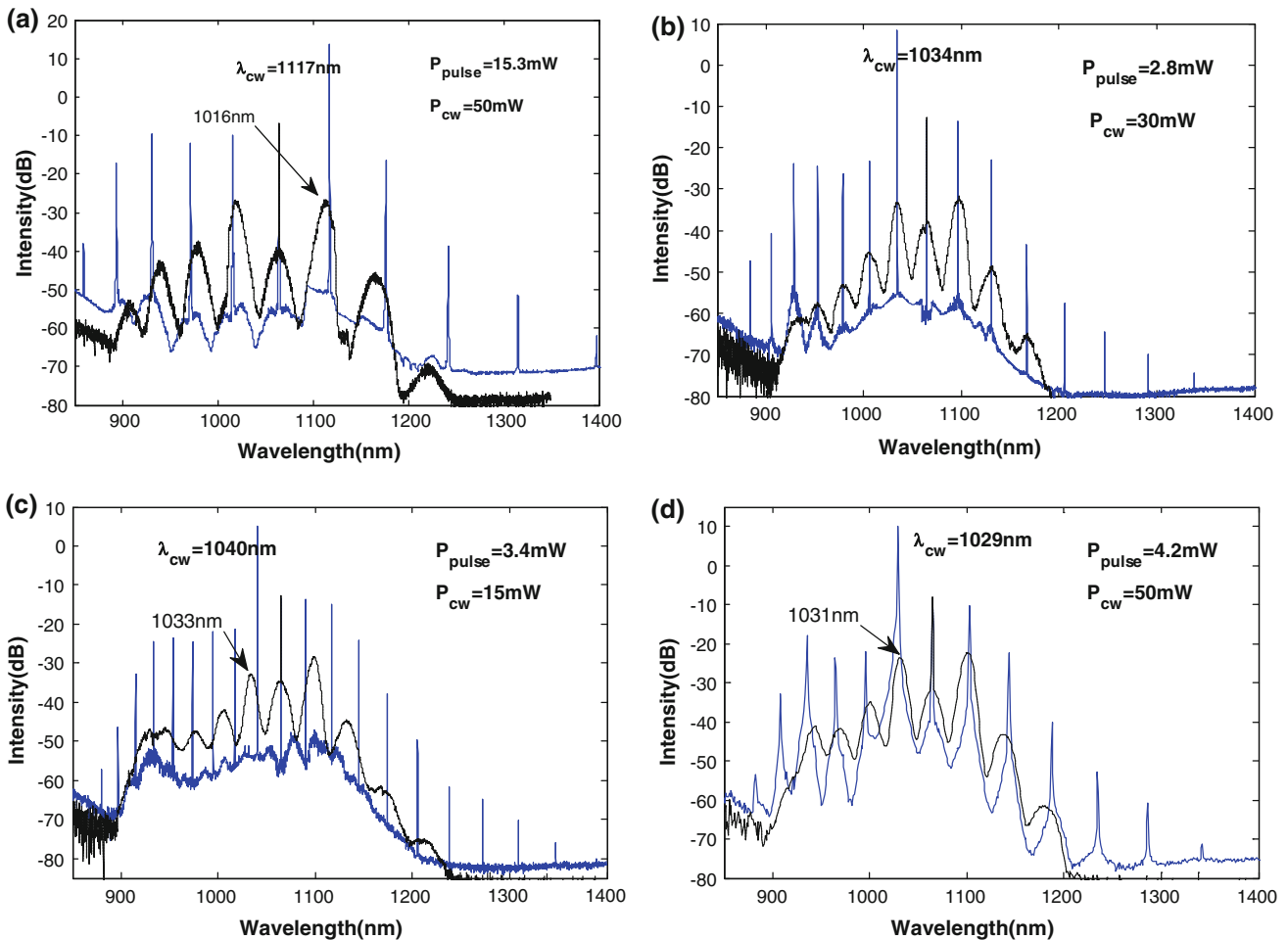


**Fig. 9** Solid lines the measured cascaded FWM sidebands in fiber B seeded by 1,117 nm (a), 1,034 nm (b), 1,040 nm (c), 1,029 nm (d). Dashed lines the spectra for only pulse pumping with the same pulse

power as that of solid lines. Fiber lengths for a–d are 0.4, 1.5, 1.5, 1.3 m, respectively

### 4 Discussion

The experimental results above demonstrate that significant effect of ZDW on the generation of cascaded FWM products. Pumping in the normal dispersion region can only get the cascaded FWM with frequency interval  $\sim 13.4$  THz in fiber A. while in fiber B the cascaded FWM frequency interval is more adjustable. To make it more convincing, we have simulated pulse pumping in the anomalous dispersion region using fiber A. In the simulations, adaptive split-step Fourier method (SSFM) was used to solve the generalized nonlinear Schrödinger equation (GNLSE) [19]. The pump pulse was selected as nonchirped Gaussian pulse ( $E(0, t) = \sqrt{P_0} \exp(-t^2/(2T_0^2))$ ) where pulse duration  $T_0 = 18$  ps (the full width at half maximum  $T_{FWHM} = 30$  ps), peak power  $P_0 = 2$  kW and center wavelength located at 1,150 nm. A CW-seed at 1,100 nm ( $\sqrt{\varepsilon_{cw} P_0} \exp(-2\pi i \Omega t)$ ) was added. The relative intensity

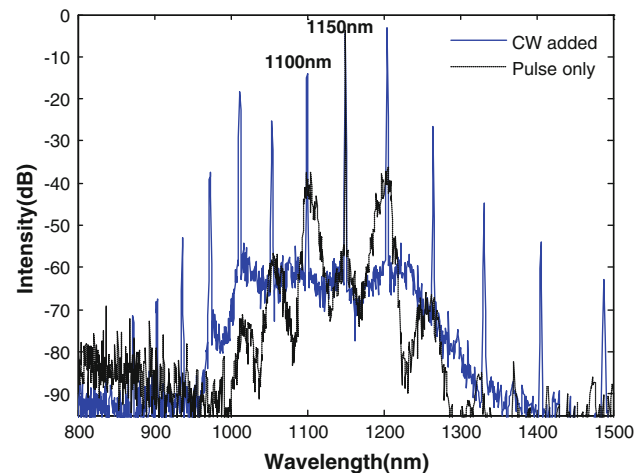


**Fig. 10** Simulation spectra of the only pulse pump at 1,150 nm (dashed line) and CW at 1,100 nm added in fiber A with fiber length of 0.8 m

$\varepsilon_{\text{CW}} = 10^{-5}$ .  $\Omega$  is the normalized frequency shift of the signal CW-seed. Its wavelength can be calculated by  $\lambda_{\text{CW}} = 1/(1/\lambda_0 + \Omega/c)$ , where  $\lambda_0$  is the center wavelength of the main pump pulse (1,150 nm) and  $c$  being the speed of light in vacuum. Noise was included in the frequency domain through one photon per mode (with random phase) spectral density on each spectral discretization bin. The results for CW signal added and only pulse pumping are compared in Fig. 10. We observe that the results are remarkably similar to that in Fig. 9 generated in fiber B.

Both the experimental and numerical results indicate that pumping in the anomalous region could be more conducive to the generation of seeded cascaded FWM with different frequency intervals. This can be explained as follows. In the case of using fiber B, MI donates for long-pulse pumping. The seeded CW signal will be enlarged as long as it locates within the MI gain bandwidth. Besides the MI gain bandwidth widens with the increasing of pumping power. So a large number of FWM sidebands will be achieved with the frequency interval determined by that between pulse and CW signal. While in the case of using fiber A, SRS dominates when pumping in the deep normal dispersion region. And the locations of Stokes or anti-Stokes peaks generated by SRS are independent of pump power. Only seeding at the Stokes or anti-Stokes peaks can we achieve efficient generation cascaded FWM or Raman sidebands.

## 5 Conclusion

We have shown cascaded FWM generation in PCFs pumping in the normal or anomalous dispersion regimes and seeded by CW signals. Experimental and numerical results demonstrated that the efficiency of generation of cascaded FWM products depends strongly on the relationship between the pulse pumping wavelength and the ZDWs of fibers. Highly nonlinear PCFs with ZDWs smaller than the pulse wavelength have been shown to be very efficient for the generation of cascaded FWM with multiple frequency intervals, which are determined by the seeding offset. In the best case, we have reported broadband generation of cascaded FWM spanning more than

500 nm. While, the PCFs with ZDWs larger than the pulse wavelength are only suitable for the generation of cascaded FWM or Raman sidebands seeded at the Stokes or anti-Stokes peaks.

**Acknowledgments** This research was supported by National Natural Science Foundation of China (Grant No: 61235008), National Natural Science Foundation (Grant No: 61077076), International Science & Technology Cooperation of China (Grant No: 2012DFG11470), Natural Science Foundation for Distinguished Young Scholars of Hunan Province (Grant No. 12JJ1010).

## References

1. G.P. Agrawal, *Nonlinear Fiber Optics*, 4th edn. (Elsevier, Amsterdam, 2007)
2. J.M. Dudley, G. Genty, S. Coen, *Rev. Mod. Phys.* **78**, 1135–1184 (2006)
3. K. Tai, A. Hasegawa, A. Tomita, *Phys. Rev. Lett.* **56**, 135–138 (1986)
4. M.H. Frosz, T. Sorensen, O. Bang, *J. Opt. Soc. Am. B* **23**, 1692–1699 (2006)
5. J.C. Travers, *J. Opt.* **12**, 113001–113020 (2010)
6. D.A. Chestnut, J.R. Taylor, *Opt. Lett.* **28**, 2512–2514 (2003)
7. A. Cerqueira Sodre, J.M. Chavez Boggio, A.A. Rieznik, H.E. Hernandez-Figueroa, H.L. Fragnito, J.C. Knight, *Opt. Express* **16**, 2816–2828 (2008)
8. J. Fatome, S. Pitois, G. Millot, *IEEE J. Quantum Elect.* **42**, 1038–1046 (2006)
9. G. Genty, J.M. Dudley, *IEEE J. Quantum Elect.* **45**, 1331–1335 (2009)
10. H. Sayinc, M. Wyszomolek, J. Chavez Boggio, R. Haynes, M. Roth, U. Morgner, J. Neumann, D. Kracht, *Appl. Phys. B Lasers Opt.* **110**, 299–302 (2013)
11. Y. Li, J. Hou, Z. Jiang, J. Leng, *Appl. Opt.* **52**, 2049–2054 (2013)
12. H.W. Chen, S.P. Chen, J. Hou, *Laser Phys.* **21**, 191–193 (2011)
13. H. Chen, S. Chen, J. Wang, Z. Chen, J. Hou, *Opt. Commun.* **284**, 5484–5487 (2011)
14. W. Yan-Bin, H. Jing, C. Zi-Lun, C. Sheng-Ping, S. Rui, L. Ying, Y. Wei-Qiang, L. Qi-Sheng, *Chin. Phys. Lett.* **28**, 74208 (2011)
15. W. Yan-Bin, X. Chun-Le, H. Jing, L. Qi-Sheng, P. Yang, C. Zi-Lun, *Acta Phys. Sin.* **60**, 014201 (2011)
16. X. Xiaoming, C. Zilun, L. Shiyao, H. Jing, J. Zongfu, *Laser Technol.* **35**, 169–173 (2011)
17. X. Xiaoming, C. Zilun, S. Guilin, C. Hongwei, L. Zhihong, H. Zhihe, H. Jing, *Acta Opt. Sin.* **31**, 0206001 (2011)
18. S.T. Sørensen, C. Larsen, U. Møller, P.M. Moselund, C.L. Thomsen, O. Bang, *J. Opt. Soc. Am. B* **29**, 2875–2885 (2012)
19. Y. Wang, C. Xiong, J. Hou, J. Cao, Y. Li, R. Song, Q. Lu, *Appl. Opt.* **50**, 2752–2758 (2011)